Rare Metal Materials and Engineering

Available online at **www.rmme.ac.cn**

Science Press

Cite this article as: Rare Metal Materials and Engineering.

ARTIC

DOI: 10.12442/j.issn.1002-185X.20240451.

Constitutive model and microstructure evolution of as-extruded Ti-6554 alloy based on temperature rise correction

Changmin Li [1,2], Hengjun Luo[1], Ning Zhao[3], Shiqi Guo[2], Minggang Wei[1], Wei Xiang[1], Mingliang Cui[1], Jing Xie[1], Liang Huang[2,*]

[1] Deyang Wanhang Die Forging Co., Ltd., China National Erzhong Group Co., Deyang 618013, P.R. China

[2] State Key Laboratory of Materials Processing and Die & Mould Technology, School of Materials Science and Engineering, Huazhong University of Science and Technology, Wuhan 430074, P.R. China

3. Western Superconducting Technologies Co., Ltd., Xi'an 710000, P.R. China

Abstract: The hot deformation behavior of as-extruded Ti-6554 alloy was investigated through isothermal compression at 700-950 °C and 0.001-1 s^{-1}. The temperature rise under different deformation conditions was calculated, and the curve was corrected. The strain compensation constitutive model of as-extruded Ti-6554 alloy based on temperature rise correction was established. The microstructure evolution under different conditions was analyzed, and the dynamic recrystallization (DRX) mechanism was revealed. The results show that the flow stress decreases with the increase of strain rate and the decrease of deformation temperature. The deformation temperature rise gradually increases with the increase of strain rate and the decrease of deformation temperature. At 700 °C/1 s^{-1}, the temperature rise reaches 100 °C. The corrected curve value is higher than the measured value, and the strain compensation constitutive model has high prediction accuracy. The precipitation of the α phase occurs during deformation in the two-phase region, which promotes the DRX process of the β phase. At low strain rate, the volume fraction of dynamic recrystallization increases with the increase of deformation temperature. The DRX mechanism includes continuous dynamic recrystallization (CDRX) and discontinuous dynamic recrystallization (DDRX).

Key words: as-extruded Ti-6554 alloy; temperature rise correction; constitutive model; microstructure evolution

The excellent mechanical properties of Ti-6Cr-5Mo-5V-4Al alloy show good potential for application in critical load-bearing components in the aviation field [1, 2]. At present, the cogging of the bar required for the load-bearing components can be carried out by hot extrusion to achieve the purpose of refining the as-cast microstructure. Because the plasticity of the material can be brought into full play under the action of three-dimensional compressive stress. For the bar after hot extrusion, it is necessary to forge to obtain parts with stable microstructure and mechanical properties [3]. Meanwhile, the microstructure after hot extrusion shows significant differences compared to that of the as-cast state. Considering that titanium alloy is a kind of difficult-to-deform material, and there are problems such as large deformation resistance and uneven microstructure in the forging process. Therefore, it is necessary to systematically study the hot deformation behavior and microstructure evolution of as-extruded titanium alloys.

It has become an effective way to analyze the flow behavior and microstructure evolution of metal materials during deformation by thermal compression experiments. Ding et al. [4] analyzed the hot deformation behavior of ZL270LF aluminum alloy, and found that the suitable processing regions are 470-530 °C/0.01-1 s^{-1}. And continuous dynamic

Received date:

Foundation item: National Key R&D Program of China (2022YFB3706901), National Natural Science Foundation of China (52274382), Key Research and Development Program of Hubei Province (2022BAA024)

Corresponding author: Liang Huang, Ph.D., Professor, E-mail: huangliang@hust.edu.cn

recrystallization (CDRX), discontinuous dynamic recrystallization (DDRX) and geometric dynamic recrystallization (GDRX) occurred during hot deformation. Feng et al. [5] analyzed the hot deformation behavior of the dual-phase Mg-Li alloy and found that the α-Mg phase was transformed into the β-Li phase in the form both of spheroidization and precipitation in the α-Mg phase. At the same time, DRX is easy to occur in the β-Li phase and is retarded in the α-Mg phase. Wang et al. [6] studied the DRX behavior of a new nickel-based superalloy and found that both DDRX and CDRX coexisted at low temperatures and low strain rates. With the increase of temperature, the CDRX became weaker, while the DDRX became stronger with the increase of strain. Cai et al. [7] studied the hot deformation behavior of equiatomic FeCrMnNi high-entropy alloy and found that the deformation microstructure was closely related to the power dissipation efficiency. When the power dissipation efficiency was 28%, the DRX volume fraction was 17.6 %. When the power dissipation efficiency increased to 38 %, the DRX volume fraction increased to 37.5 %. Shi et al. [8] analyzed the high temperature deformation behavior and recrystallization mechanism of Ti-55511 alloy and found that with the increase of deformation temperature, the DRX mechanism gradually transformed from DDRX to CDRX.

In the process of hot deformation, the stress-strain curve is an important means to reflect the flow stress of the material and to measure the processing performance of the material. The heat generated during the deformation process of the sample, especially at high strain rates, is difficult to dissipate effectively, resulting in a significant temperature rise inside the sample [9]. This will cause the measured value of the flow stress to deviate from the true value. Therefore, in order to deeply analyze the high temperature deformation behavior of titanium alloy and accurately obtain the stress-strain curve during hot compression, it is necessary to consider the influence of temperature rise on the curve. At present, researchers have carried out temperature rise correction in AZ31 magnesium alloy [10], Ti-55531 alloy [11], 300M steel [12] and other materials.

In previous studies, the hot extrusion process of Ti-6554 has been extensively analyzed [13]. At the same time, the researchers have also delved into the hot deformation behavior of the as-forged Ti-6554 alloy [14-16]. Considering that the microstructure after extrusion is significantly different from that of as-cast and as-forged, it is necessary to analyze the hot deformation behavior of as-extruded alloys. Therefore, in this study, the hot deformation behavior of as-extruded Ti-6554 alloy was analyzed, the deformation temperature rise under different conditions was calculated, the stress-strain curve was corrected, and the constitutive equation was established. In addition, the microstructure evolution and DRX mechanism under different conditions were also analyzed.

1 Experiment

The material used in the present study was an extruded Ti-6554 alloy bar with a diameter of 70mm. During the extrusion process, the extrusion speed is 40mm/s, the extrusion temperature is 1100 °C, and the extrusion ratio is 10[13]. The chemical composition (wt.%) is: 6.2Cr-5.3Mo-5.5V-4.0Al-0.17O-0.09N-(Bal.)Ti and its initial microstructure is shown in Fig 1[13]. The phase transition point for this alloy is 785±5°C. The samples were cylinders of Φ8 mm×12 mm by wire cutting. The hot compression test was carried out on a Gleeble3800 thermal simulator, and the deformation temperatures were 700-950 °C, and strain rates were 0.001-1 s^{-1}. In order to reduce friction, tantalum sheets were placed between the sample and the mold. Before hot compression, the samples were heated to the deformation temperature at a rate of 10 °C/s to and held for 5 min. After hot compression, the samples were immediately water-cooled to obtain the deformed structure. Subsequently, the sample was cut along the compression direction by a wire cutting machine. The samples were mechanically ground and polished, followed by etching at room temperature in a solution of 2ml hydrofluoric acid, 10ml nitric acid and 88ml water. Microstructure characterization was performed on an optical microscope. For EBSD, the samples were mechanically ground and then electropolished in the mixed solution of 70ml methanol, 20ml ethylene glycol and 10ml perchloric acid. EBSD scanning was performed on an OXFORD-NordlysMax system with a step of 0.5-1 μm.

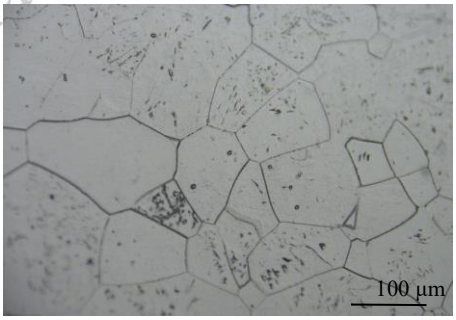

Fig 1 The initial microstructure of as-extruded Ti-6554 alloy

2 Results and Discussion

2.1 Stress-strain curve

Fig 2 shows the stress-strain curves under different conditions. Work hardening is dominant in the early deformation stage, and dislocation density increases rapidly. At the same time with the increase of strain, the flow stress increases rapidly to the peak. Subsequently, various softening mechanisms appear, such as DRX, dynamic recovery (DRV) and so on. The flow stress shows an obvious downward trend. When the work hardening and dynamic softening reach equilibrium, the flow curve reaches a stable state. In addition, it can be found that the flow stress of the as-extruded Ti-6554 alloy is significantly affected by the deformation parameters, and gradually decreases with the increase of strain rate and the decrease of deformation temperature. At 700 °C/0.001 s^{-1}, the decrease of the curve is very obvious, while the decrease of the curve in the single-phase region is very small. This shows that the softening mechanism in the two-phase region is different from that in the single-phase region.

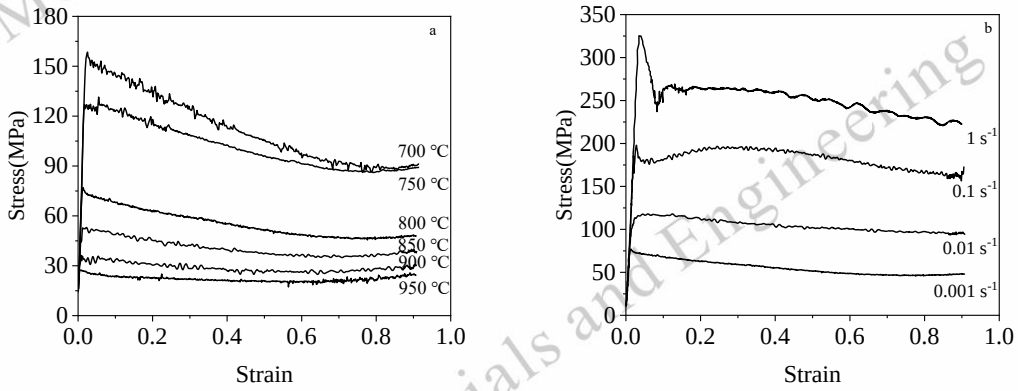

Fig 2 The stress-strain curves of as-extruded Ti-6554 alloy under different conditions: (a) 0.001 s^{-1}; (b) 800 ℃

3.2 Deformation heat effect

The deformation heat effect is a common phenomenon in the hot deformation process of titanium alloy. The deformation heat effect will cause the actual deformation temperature of titanium alloy to be higher than the heating temperature, which is beneficial to promote dislocation rearrangement and reduce dislocation density [17]. The increase of deformation temperature can further promote DRX and DRV, and enhance the softening effect of titanium alloy. In addition, due to the poor thermal conductivity of titanium alloy, the deformation temperature rise will lead to the generation of local plastic flow [18]. At present, under the same deformation temperature and deformation amount, the influence of deformation heat effect on the flow stress of titanium alloy mainly depends on the strain rate. The temperature rise in the deformation process is calculated by the following formula [10, 19]:

$$\begin{cases} \Delta T = \dfrac{0.95\eta \int_0^{\varepsilon} \sigma d_{\varepsilon}}{\rho c} \\ \eta = 0.316 \log(\dot{\varepsilon}) + 0.95\ 10^{-3} \end{cases} \quad (1)$$

where ΔT is deformation temperature rise, η is adiabatic correction factor, $\int_0^{\varepsilon} \sigma d_{\varepsilon}$ is the area under the uncorrected stress and strain curves, ρ is materials density (4.5g/cm^3), c is specific heat capacity (0.52 J/(g·K)). In this paper, the deformation heat under different conditions is calculated, as shown in the

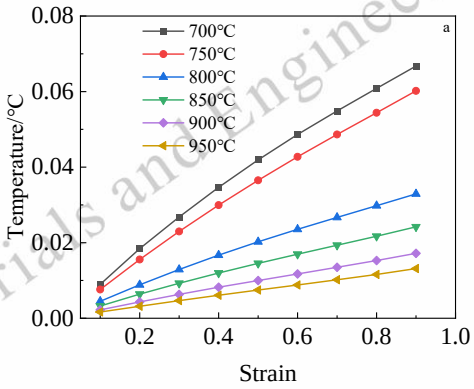

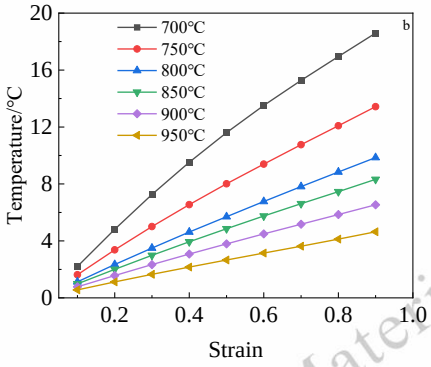

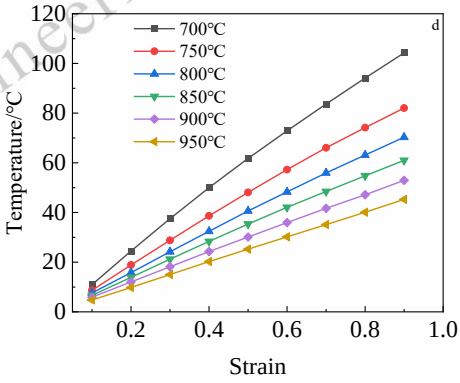

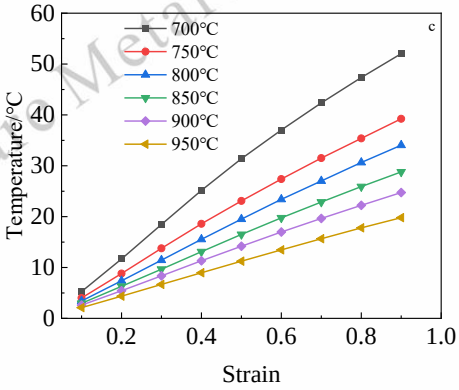

Fig 3. The deformation temperature rise gradually increases with the increase of strain rate and the decrease of deformation temperature. At 700°C/1 s^{-1}, the temperature rise reaches 100°C. Xu et al. [20] found that the temperature rise of Ti-17 alloy at 780°C/10 s^{-1} was 80 °C, and the change trend of temperature rise was also consistent with this paper. Therefore, at 700°C/1s^{-1}, the reason for the obvious softening of the stress-strain curve may be related to the deformation heat effect.

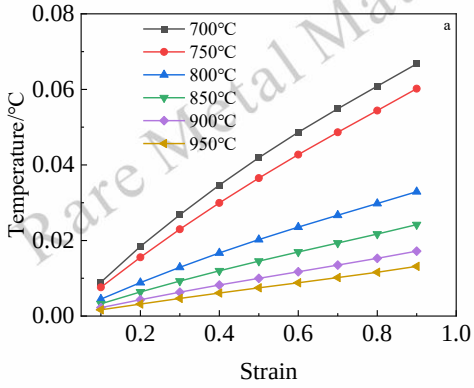

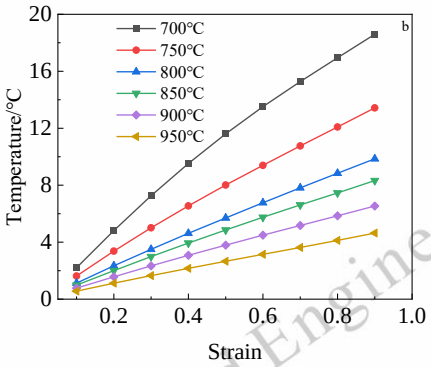

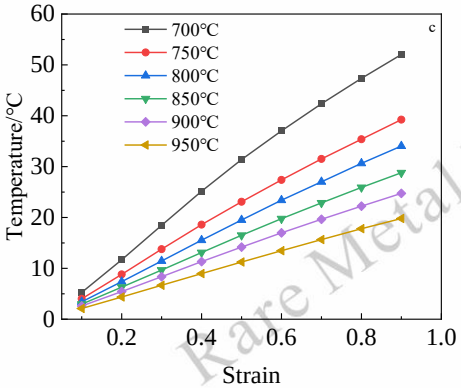

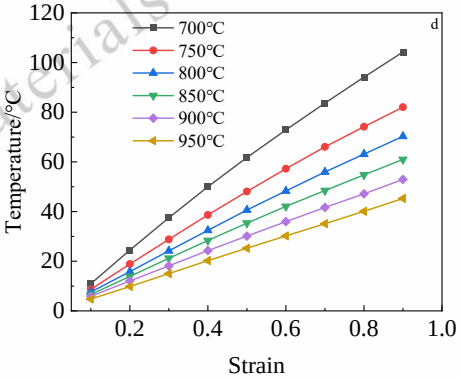

Fig 3 Temperature rise of as-extruded Ti-6554 alloy under different conditions: (a) 0.001 s^{-1}; (b) 0.01 s^{-1}; (c) 0.1 s^{-1}; (d) 1 s^{-1}

3.3 Stress-strain curve correction

At high strain rates, due to the short deformation time, the thermocouple can only measure the temperature of the sample surface, and the Gleeble system is difficult to adjust the temperature change, which significantly reduces the deformation resistance. Therefore, it is necessary to correct the curve. At present, at a given strain and strain rate, the stress-strain curve should be corrected by the following formula [11]:

$$\bar{\sigma} = \sigma - \frac{d\sigma}{dT}\Big|_{\dot{\varepsilon},\varepsilon} \Delta T \quad (2)$$

where T is deformation temperature, σ is true stress (corrected), $\bar{\sigma}$ is the measured stress (uncorrected). Fig 4 shows the comparison between the corrected curve and the uncorrected curve. It can be found that there is no significant difference between the measured value and the corrected value at a low strain rate. Therefore, the deformation heat effect at a low strain rate can be ignored. At high strain rates, the corrected value is significantly higher than the measured value, which means that temperature rise can effectively promote flow softening (Fig 4(d)).

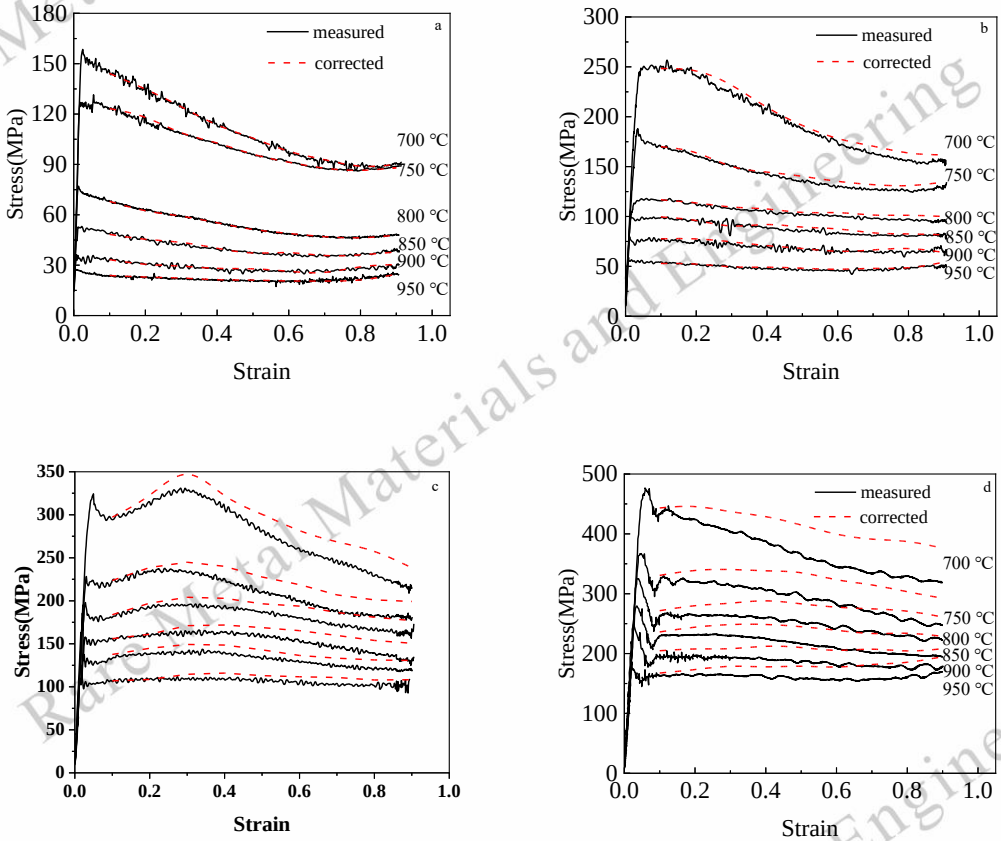

Fig 4 Comparison of stress-strain curves before and after correction under different conditions: (a) 0.001 s^{-1}; (b) 0.01 s^{-1}; (c) 0.1 s^{-1}; (d) 1 s^{-1}

3.4 Constitutive equation

The effect of strain on flow stress is not as significant as that of strain rate and deformation temperature. Therefore, the influence of strain on flow stress can be ignored, and it is proposed that the relationship between flow stress and strain rate and deformation temperature in steady-state flow stage conforms to three Arrhenius models, namely exponential function type, power function type and hyperbolic sine type. Their expressions are as follows [21]:

$$\dot{\varepsilon}\exp(Q/RT) = A_1\exp(n_1\sigma) \quad (3)$$

$$\dot{\varepsilon}\exp(Q/RT) = A_2\exp(\beta\sigma) \quad (4)$$

$$\dot{\varepsilon}\exp(Q/RT) = A\sinh(\alpha\sigma)^n \quad (5)$$

where $\dot{\varepsilon}$ represents the strain rate, Q represents the thermal deformation activation energy, R represents the gas constant, σ represents the flow stress, T represents the deformation temperature, n_1 and n represent material parameters related to the strain rate sensitivity index, and A, A_1, A_2 and α represent material constants. In order to calculate the parameters in the above equations, take the natural logarithm of the Eqs. *(3)*-*(5)*:

$$\ln\dot{\varepsilon} = lnA_1 + n_1 ln\sigma - Q/RT \quad (6)$$

$$ln\dot{\varepsilon} = lnA_2 + \beta\sigma - Q/RT \quad (7)$$

$$ln\dot{\varepsilon} = lnA + \mathrm{nln}[\sinh(\alpha\sigma)] - Q/RT \quad (8)$$

According to Eq. *(6)* and Eq.*(7)*, it can be found that $\ln\dot{\varepsilon}$ has an obvious linear relationship with $ln\sigma$ and σ, respectively. Subsequently, the peak stress in the stress-strain curve is selected for linear fitting, and the results are shown in the Fig 5 (a)(b). n1 and β are the average of the reciprocal of the slope of the curve in the figure. The calculated values of n_1 and β are 4.8833 and 0.031, respectively. The value of α can be calculated by the following formula:

$$\alpha = \beta/n_1 \quad (9)$$

According to Eq. *(9)*, the value of α under peak stress can be calculated to be 0.006347. In addition, according to Eq. *(8)*, the thermal activation energy Q can be calculated by the following formula:

$$Q = Rnk = Rn \cdot \left(\frac{\partial ln sinh(\alpha\sigma_p)}{\partial(1/T)}\right)_{\dot{\varepsilon}} \quad (10)$$

where n is the stress index, which is defined as:

$$n = \left(\frac{\partial ln\dot{\varepsilon}}{\partial ln[sinh(\alpha\sigma)]}\right)_T \quad (11)$$

According to the Eq. *(10)* and Eq. *(11)*, the average values of the slopes of $\ln[\sinh(\alpha\sigma_p)]$ - $\ln\dot{\varepsilon}$ and $\ln[\sinh(\alpha\sigma_p)]$-1/T can be determined (Fig 5 (c)(d)), and then the values of Q and n are calculated to be 233.514kJ/mol and 3.384, respectively. In addition, it was noted that the effects of deformation temperature and strain rate on the hot deformation behavior of the alloy can be expressed by the Zener-Hollomon parameter:

$$\mathrm{Z} = \dot{\varepsilon}\exp(\mathrm{Q/RT}) = A[sinh(\alpha\sigma)]^n \quad (12)$$

Taking the natural logarithm of both sides of the Eq. *(12)*:

$$\ln\mathrm{Z} = \ln\dot{\varepsilon} + \mathrm{Q/RT} = \ln A + nln[sinh(\alpha\sigma)] \quad (13)$$

According to Eq. *(13)*, it can be determined that there is a clear linear relationship between lnZ and $ln[sinh(\alpha\sigma)]$, and the fitting results are shown in the Fig 6. The intercept in the figure is the value of lnA, which can be determined as 21.65. Therefore, the constitutive model of as-extruded Ti-6554 alloy under peak stress after temperature rise correction can be expressed as:

$$\dot{\varepsilon} = 2.533 \times 10^9\left[sinh\left(0.006347\sigma_p\right)\right]^{3.384} exp(-233514/RT) \quad (14)$$

It can be seen from Fig 4 that the strain significantly affects the flow stress. In fact, both the material constants and the thermal deformation activation energy are affected by the strain and follow a polynomial relationship [22-24]. Obviously, the Arrhenius constitutive model (Eq. *(14)*) does not consider the effect of strain on the flow stress, which may lead to the low accuracy of the constitutive equation. Therefore, the Arrhenius constitutive model must be modified by strain compensation to improve its accuracy and achieve better predictability. The material constants and thermal deformation activation energy under different strains are shown in Fig 7. It can be observed that the material constants and thermal activation energy change significantly with strain. According to reference [24], the relationship between true strain and material constants can be fitted by a fifth-order polynomial, as shown in Eq. *(15)*, with the coefficients of the polynomial function presented in Table 1.

$$\mathrm{K} = c_0 + c_1\varepsilon + c_2\varepsilon^2 + c_3\varepsilon^3 + c_4\varepsilon^4 + c_5\varepsilon^5 + \cdots \quad (15)$$

After calculating the material constants and thermal activation energy under different strains, the strain-compensated Arrhenius constitutive model can be used to predict as follows:

$$\sigma = \frac{1}{\alpha_{(\varepsilon)}}\ln\left\{\left(\frac{\dot{\varepsilon}\exp\left[\mathrm{Q}_{(\varepsilon)}/\mathrm{RT}\right]}{\mathrm{A}_{(\varepsilon)}}\right)^{\frac{1}{\mathrm{n}_{(\varepsilon)}}} + \left[\left(\frac{\dot{\varepsilon}\exp\left[\mathrm{Q}_{(\varepsilon)}/\mathrm{RT}\right]}{\mathrm{A}_{(\varepsilon)}}\right)^{\frac{2}{\mathrm{n}_{(\varepsilon)}}} + 1\right]^{\frac{1}{2}}\right\} \quad (16)$$

Fig 8 is the comparison between the predicted flow stress and the experimental flow stress. It can be seen that the predicted values based on the constitutive model are basically consistent with the experimental values. Furthermore, the prediction accuracy is quantitatively analyzed by correlation

coefficient (R^2) and average absolute error (Δ) as follows[23]:

$$R^2 = \frac{\sum_{i=1}^{n}(\sigma_E - \overline{\sigma}_E)(\sigma_p - \overline{\sigma}_p)}{\sqrt{\sum_{i=1}^{n}(\sigma_E - \overline{\sigma}_E)(\sigma_p - \overline{\sigma}_p)^2}} \quad (17)$$

$$\Delta(\%) = \frac{1}{n}\sum_{i=1}^{n}\left|\frac{\sigma_E^i - \sigma_p^i}{\sigma_E^i}\right| \times 100 \quad (18)$$

where σ_E represents experimental flow stress, σ_p represents predicted flow stress, n represents the total amount of data. The linear correlation coefficient between the predicted and experimental values is 0.988 (Fig 9), and the absolute value of the average relative error is 5.75%. This shows that the hot deformation constitutive model of as-extruded Ti-6554 alloy considering strain compensation has high accuracy and can be used to predict the flow stress of the alloy in the hot deformation.

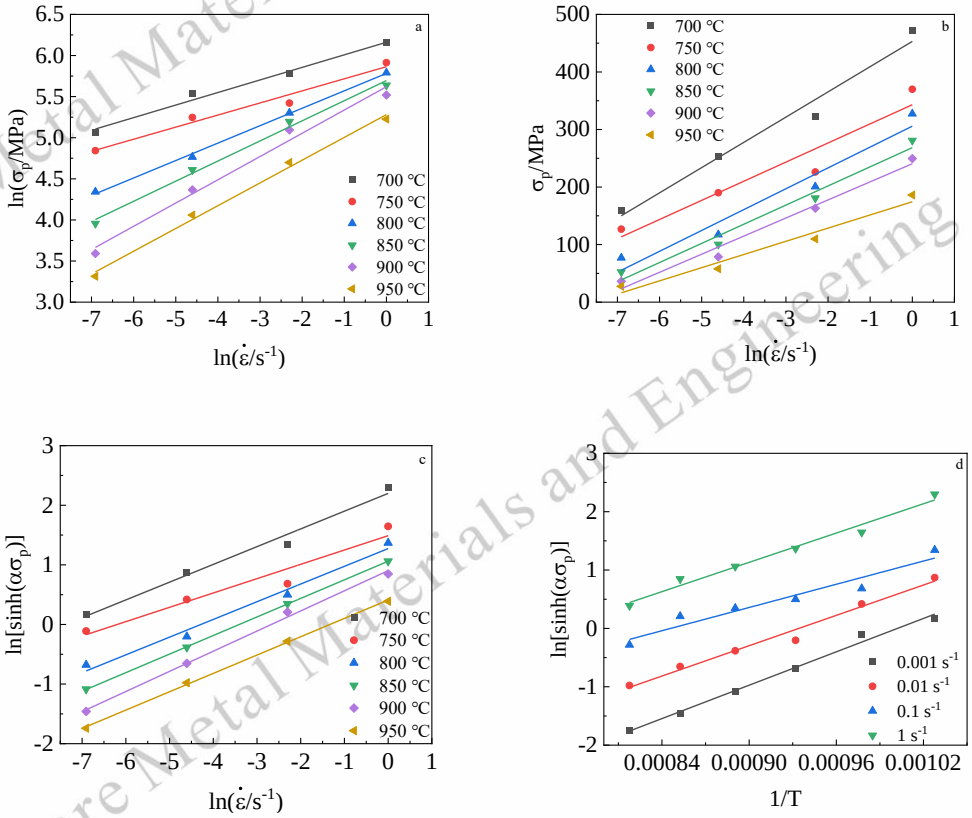

Fig 5 Relationships of (a) $ln\sigma$- $ln\dot{\varepsilon}$; (b) σ-$ln\dot{\varepsilon}$; (c) ln [sinh ($\alpha\sigma_p$)]-$ln\dot{\varepsilon}$; (d) ln [sinh ($\alpha\sigma_p$)]-1/T

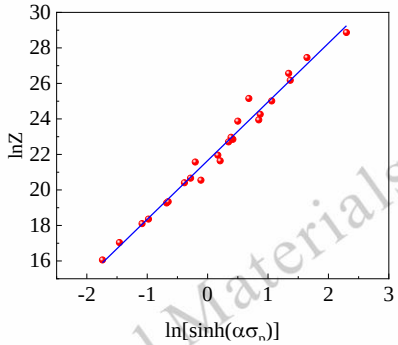

Fig 6 Relationships of lnZ and $ln[sinh(\alpha\sigma)]$

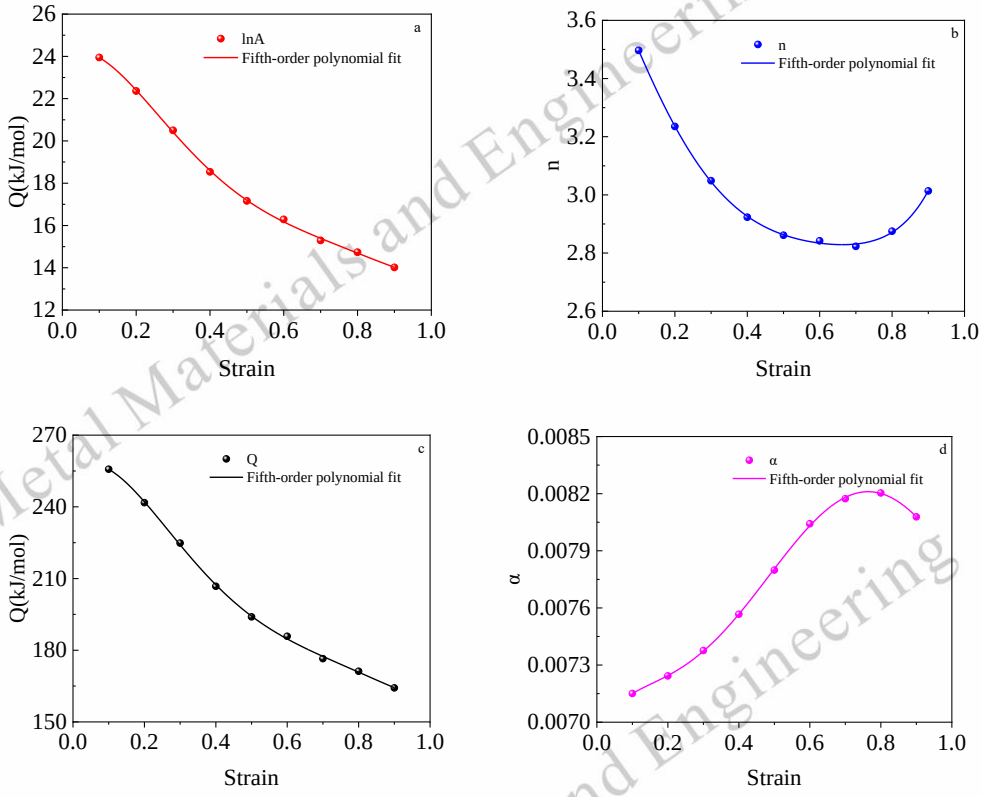

Fig 7 The variation of material constants and thermal activation energy with strain

Table 1 Polynomial fitting results of α, n, Q and lnA of Ti-6554 alloy in two-phase region

	α (MPa^{-1})	n	Q (kJ/mol)	lnA
c_0	0.00698	3.79019	254.62209	12.86044
c_1	0.00276	-2.86484	131.3988	-159.7251
c_2	-0.01422	-2.35929	-1495.11767	341.67247
c_3	0.04543	19.03922	3143.96135	-305.33547
c_4	-0.05249	-26.88646	-2772.77896	100.15224
c_5	0.01941	12.65748	897.13047	12.86044

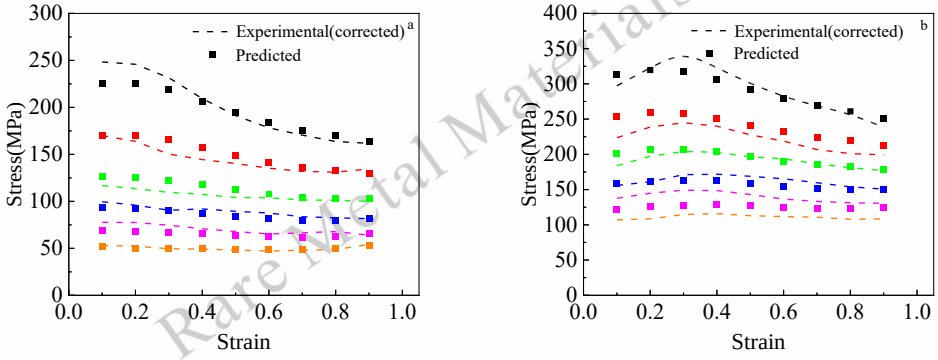

Fig 8 Comparison of experimental and predicted values: (a) 0.01 s^{-1}, (b) 0.1 s^{-1}

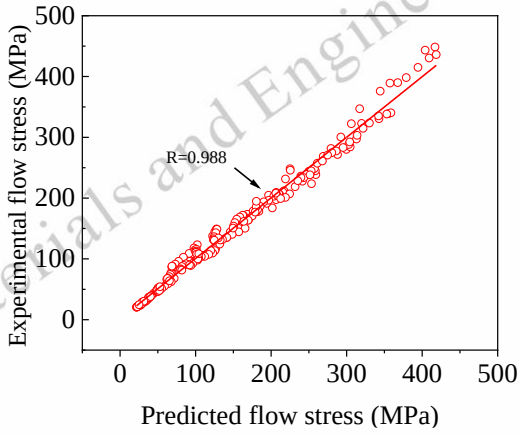

Fig 9 Correlation between experimental and predicted values

3.5 Microstructure analysis

Fig 10 shows the microstructure of as-extruded Ti-6554 alloy under all deformation conditions. It can be found that some α phases precipitate at low strain rates in the two-phase region. With the increase of strain rate, the volume fraction of the α phase decreases significantly, and there is no obvious change rule. This shows that the precipitation behavior of the α phase is not only affected by the strain rate, this phenomenon has also been reported in other studies [25]. Notably, the original β grains become distinctly elongated at lower temperatures and higher strain rates, indicating that DRV is the predominant deformation mechanism. Meanwhile, it should be noted that flow localization occurs at 700 °C/1 s^{-1}. This is related to the deformation temperature rise at low temperatures and high strain rate, which further illustrates the necessity of temperature rise correction. In the single-phase region, obvious grain boundary bulging occurs at low strain rates, and many DRX grains are also observed. The increase of temperature provides sufficient driving force for DRX. At the same time, a low strain rate is beneficial to the nucleation and growth of DRX grains. With the increase of deformation temperature, the volume fraction and grain size of DRX gradually increase. As the strain rate increases, the original β grains are also elongated. Different from low temperature, the grain boundary is serrated at 900 °C and 950 °C.

Then, EBSD is used to analyze the microstructure evolution in the deformation process of the two-phase region. Fig 11 shows the EBSD results at 700 °C with different strain rates. Black is a large angle grain boundary, blue is a β phase, and red is a α phase. The α phase precipitates at the grain boundary and interior of elongated β grain. It should be noted that some very fine DRX grains are also found in the Fig 11 (a). Some studies have pointed out that during the deformation process, the incoherent phase interface can hinder the dislocation movement [26, 27] thus providing sufficient driving energy for the β-phase DRX process. Furthermore, the dislocation density will increase significantly at a lower deformation temperature, which will further provide energy for the DRX process. Therefore, the curve decreases significantly at low strain rate in the two-phase region (Fig 2 (a)).

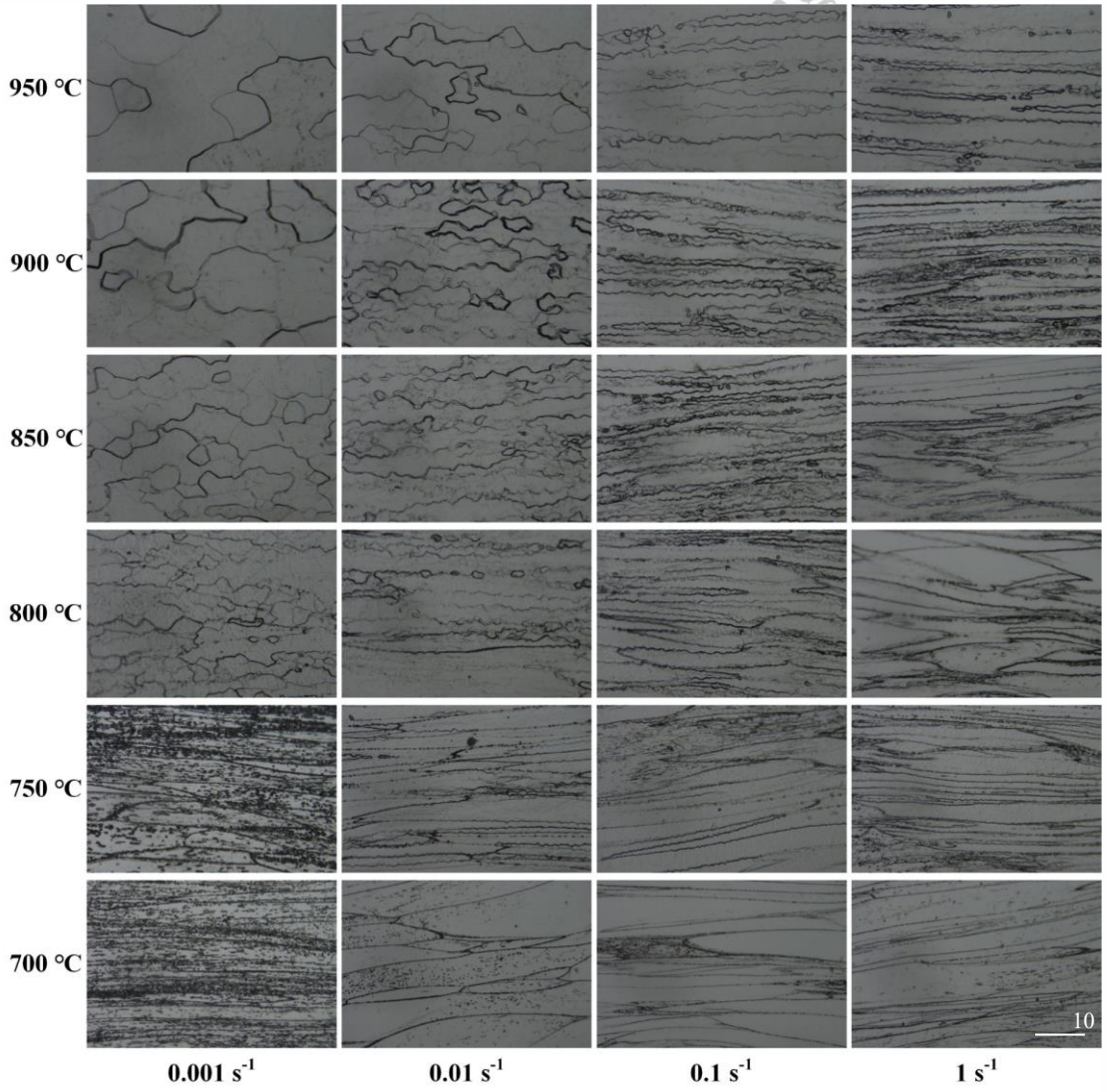

Fig 10 Microstructure of as-extruded Ti-6554 alloy under different conditions

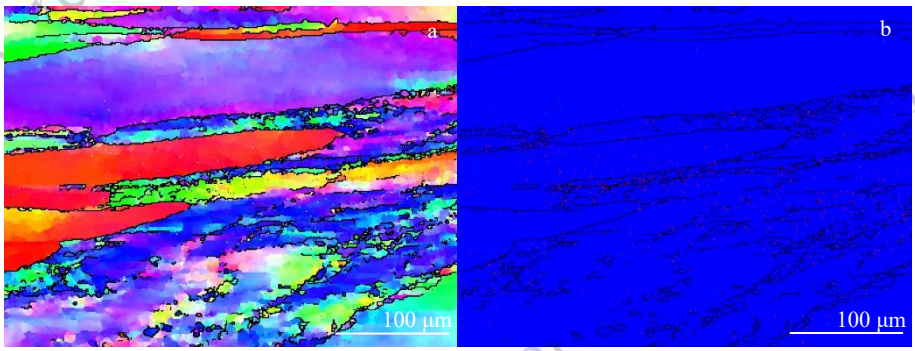

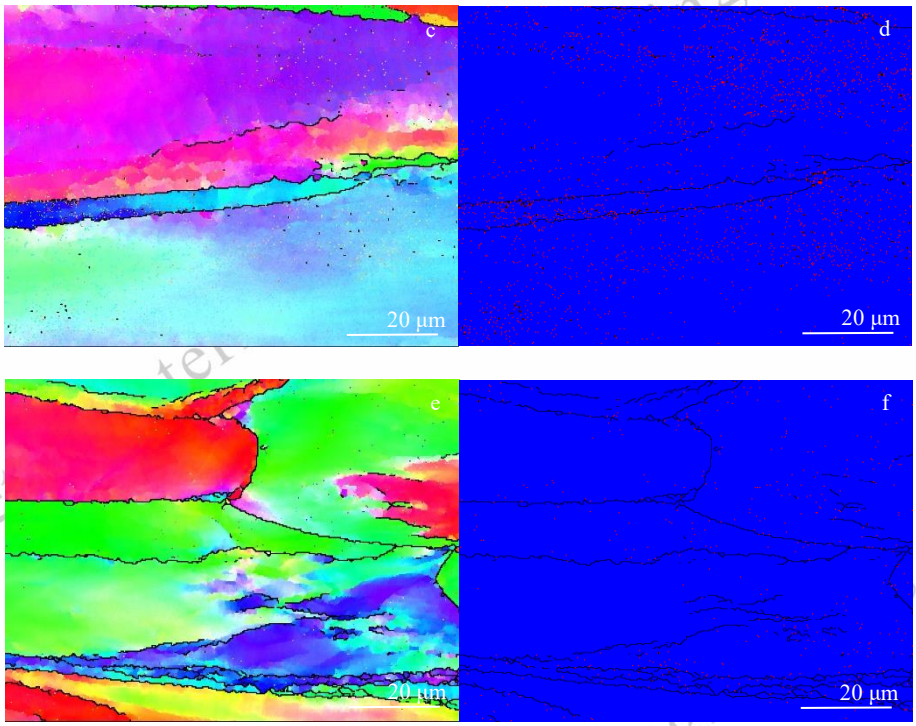

Fig 11 EBSD results: IPF maps of (a) 700 ℃/0.001 s^{-1}; (c) 700 ℃/0.01 s^{-1}; (e) 700 ℃/1 s^{-1}; phase distribution maps of (b) 700 ℃/0.001 s^{-1}; (d) 700 ℃/0.01 s^{-1}; (f) 700 ℃/1 s^{-1}

3.6 Dynamic recrystallization behavior

Fig 12 shows the EBSD results at 900 °C /0.001 s^{-1} and 900 °C 0.1 s^{-1}. Black is a large angle grain boundary, and white is a low angle grain boundary. At 900 °C /0.001 s^{-1}, the lower strain rate is beneficial to the migration of grain boundaries, and most grain boundaries show obvious bulging, as shown in Fig 12 (a). This is consistent with the results in Fig 10. The grain boundary bulging can be regarded as the nucleation stage of DDRX. This is the phenomenon of strain-induced grain boundary migration, which belongs to the DDRX process [28, 29]. This is a strain-induced grain boundary migration mechanism, which belongs to a typical DDRX process. The proportion of LAGBs in the sample is very low. At the same time, according to the cumulative misorientation inside the grains, it can be found that the cumulative orientation inside the grains does not exceed 15° (Fig 13 (a)(b)). A similar phenomenon has been observed in previous studies [30-32]. and the grain boundaries gradually become straight, as shown in Fig 12 (b). Higher strain rate promotes dislocation proliferation, but reduces the time of dynamic recrystallization nucleation and growth. According to the cumulative misorientation in Fig 13 (c), it can be determined that CDRX occurs during the deformation process. In the existing research, the 10°-15° indicates the occurrence of CDRX [33]. CDRX can be regarded as the recrystallization mechanism through progressive subgrain rotation. Meanwhile, DDRX also occurs under this condition (Fig 13 (d)).

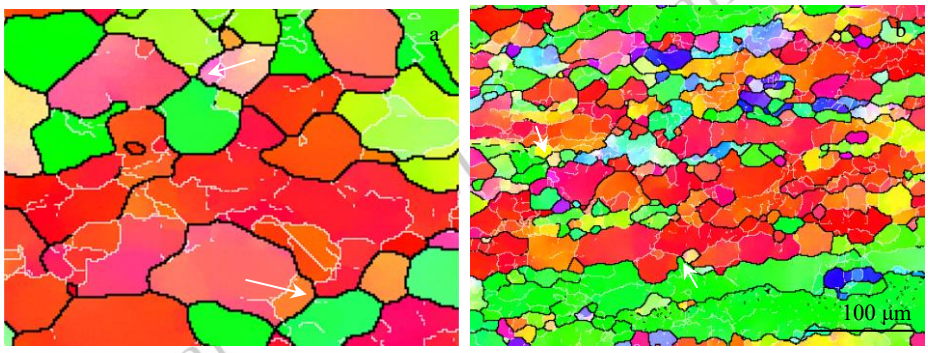

Fig 12 EBSD results: (a) 900 °C /0.001 s^{-1}; (b) 900 °C 0.1 s^{-1}

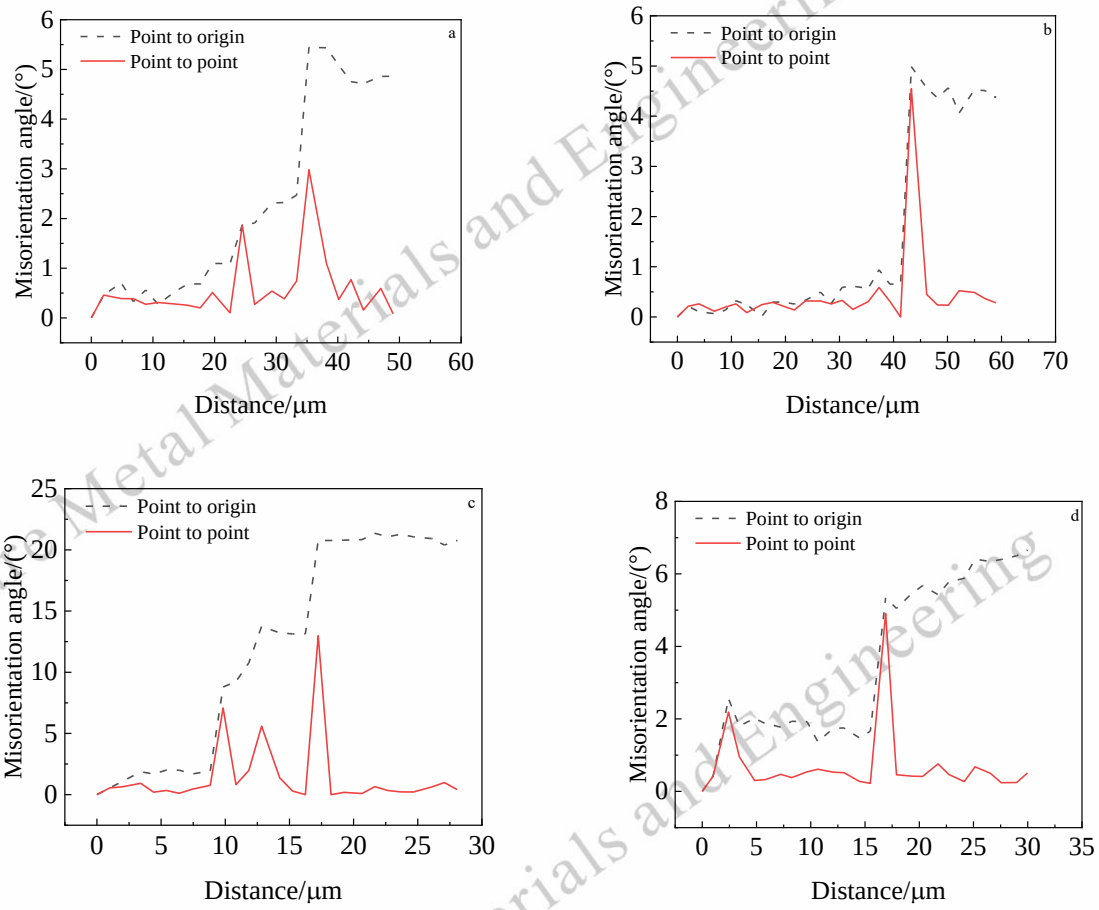

Fig 13 Misorientation angle along the arrows marked in Fig 12: (a) L1; (b) L2; (c) L3; (d) L4

3 Conclusions

1) The flow stress decreases with the increase of strain rate and the decrease of deformation temperature. The deformation temperature rise is more significant at a high strain rate. At 700 °C/1s^{-1}, the temperature rise reaches 100 °C.

2) The corrected curve value is higher than the measured value. The constitutive model of as-extruded Ti-6554 alloy was established:

$$\dot{\varepsilon} = 2.533 \times 10^{9}\left[sinh\left(0.006347\sigma_{p}\right)\right]^{3.384} exp(-233514/RT)$$

3) The precipitation of the α phase occurs during deformation in the two-phase region, which promotes the DRX process of the β phase.

4) The DRX mechanism includes continuous dynamic recrystallization (CDRX) and discontinuous dynamic recrystallization (DDRX).

References

1 Li Tong, Kent Damon, Sha Gang et al. Acta Materialia[J], 2016, 106: 353-366

2 Wu Chuan, Zhou Yu jie, Liu Bin. Materials Science and Engineering: A[J], 2022, 838: 142745

3 Zhang S H, Xu Y, Shang Y L et al. Journal of Materials Science & Technology[J], 2001, 17(1): 113-114

4 Ding Wanwu, Chen Shihao, Hu Liwen et al. Rare Metal Materials and Engineering[J], 2023, 52(12): 4086-4098

5 Feng Yinghao, Sun Chaoyang, Xu Sinuo et al. Rare Metal Materials and Engineering[J], 2023, 52(4): 1227-1237

6 Wang Xingmao, Ding Yutian, Bi Zhongnan et al. Rare Metal Materials and Engineering[J], 2023, 52(02): 517-526

7 Cai Zhen, Wu Tiandong, Wei Na et al. Rare Metal Materials and Engineering[J], 2022, 51(11): 4051-4058

8 Shi S X, Ge J Y, Lin Y C et al. Materials Science and Engineering: A[J], 2022, 847: 143335

9 Sun J Z, Li M Q, Li H. Materials Science and Engineering: A[J], 2017, 697: 132-140

10 Ding Xiaofeng, Zhao Fuqiang, Shuang Yuanhua et al. Journal of Materials Processing Technology[J], 2020, 276: 116325

11 Wu C, Huang L, Li C M. Materials Science and Engineering: A[J], 2020, 773: 138851

12 Zhao Mingjie, Huang Liang, Li Changmin et al. Materials Science and Engineering: A[J], 2021, 810: 141031
13 Guo Shiqi, Huang Liang, Li Changmin et al. The International Journal of Advanced Manufacturing Technology[J], 2024, 131(7): 4233-4252
14 Li Changmin, Huang Liang, Zhao Mingjie et al. Journal of Alloys and Compounds[J], 2022, 924: 166481
15 Li C M, Huang L, Zhao M J et al. Materials Science and Engineering: A[J], 2021, 814: 141231
16 Long S., Xia Y. F., Wang P. et al. Journal of Alloys and Compounds[J], 2019, 796: 65-76
17 Gao Pengfei, Fu Mingwang, Zhan Mei et al. Journal of Materials Science & Technology[J], 2020, 39: 56-73
18 Li Changmin, Huang Liang, Li Chenglin et al. Rare Metals[J], 2022, 41(5): 1434-1455
19 Jia Zhi, Yu Lidan, Wei Baolin et al. Rare Metal Materials and Engineering[J], 2022, 51(2): 461-468
20 Xu J W, Zeng W D, Zhou D D et al. Journal of Alloys and Compounds[J], 2018, 767: 285-292
21 Liu Anjin, Wang Lin, Cheng Xingwang et al. Rare Metal Materials and Engineering[J], 2021, 50(12): 4201-4208
22 Wen DongXu, Yue TianYu, Xiong YiBo et al. Materials Science and Engineering: A[J], 2020: 140491
23 Wang Yitao, Li Jianbo, Xin Yunchang et al. Materials Science and Engineering: A[J], 2019, 768: 138483
24 Dong Entao, Yu Wei, Cai Qingwu et al. Materials Science and Engineering: A[J], 2019, 764: 138228
25 Matsumoto Hiroaki, Kitamura Masami, Li Y P et al. Materials Science and Engineering: A[J], 2014, 611: 337-344
26 Lin Y C, Huang J, He D G et al. Journal of Alloys and Compounds[J], 2019, 795: 471-482
27 Li C M, Huang L, Zhao M J et al. Materials Science and Engineering: A[J], 2022, 850: 143571
28 Wang M J, Sun C Y, Fu M W et al. Journal of Alloys and Compounds[J], 2020, 820: 153325
29 Zhao Q Y, Yang F, Torrens R et al. Materials Characterization[J], 2019, 149: 226-238
30 Zhao Juan, Zhong Jie, Yan Fei et al. Journal of Alloys and Compounds[J], 2017, 710: 616-627
31 Zhong Liwei, Gao Wenli, Feng Zhaohui et al. Journal of Materials Science & Technology[J], 2019, 35(10): 2409-2421
32 Zang Qianhao, Yu Huashun, Lee Yun-Soo et al. Materials Characterization[J], 2019, 151: 404-413
33 Zang Qianhao, Yu Huashun, Lee Yun-Soo et al. Journal of Alloys and Compounds[J], 2018, 763: 25-33

基于温升修正的挤压态 Ti-6554 合金本构模型和微观组织演化

李昌民[1,2]，罗恒军[2]，赵宁 3，郭士琦[2]，魏明刚[2]，向伟[1]，崔明亮[2]，谢静[1]，黄亮[2]

(1. 中国第二重型机械集团德阳万航模锻有限责任公司，四川 德阳 618013)

(2. 华中科技大学，材料科学与工程学院，材料成形与模具技技术全国重点实验室，湖北 武汉 430074)

(3. 西部超导材料科技股份有限公司，陕西 西安 710000)

摘　要：在 700-950°C、0.001~1 s^{-1} 的等温压缩条件下，研究了挤压态 Ti-6554 合金的热变形行为。计算了不同变形条件下的温升，对曲线进行了温升修正，建立了基于升温修正的挤压态 Ti-6554 合金的应变补偿本构模型。分析了不同条件下的微观组织演化规律，揭示了动态再结晶机制。结果表明流动应力随着应变速率的增加和变形温度的降低逐渐下降。变形温升随着应变速率的增加和变形温度的降低逐渐增加，在 700℃/1 s^{-1} 时，温升达到 100℃。修正后的曲线值高于测量值，应变补偿本构模预测精度较高。在两相区变形时析出了 α 相，进而促进了 β 相的 DRX 过程。低应变速率下，随着变形温度升高到，动态再结晶体积分数增加。DRX 机制包含连续动态再结晶和非连续动态再结晶。

关键词：挤压态Ti-6554合金; 温升修正; 本构模型; 微观组织演化

作者简介：李昌民，男，1994 年生，博士，中国第二重型机械集团德阳万航模锻有限责任公司，四川 德阳 618013，E-mail: lcm940214@126.com